

This is the accepted manuscript made available via CHORUS. The article has been published as:

Surface terminations and layer-resolved tunneling spectroscopy of the 122 iron pnictide superconductors

Ang Li, Jia-Xin Yin, Jihui Wang, Zheng Wu, Jihua Ma, Athena S. Sefat, Brian C. Sales, David G. Mandrus, Michael A. McGuire, Rongying Jin, Chenglin Zhang, Pengcheng Dai, Bing Lv, Ching-Wu Chu, Xuejin Liang, P.-H. Hor, C.-S. Ting, and Shuheng H. Pan

Phys. Rev. B **99**, 134520 — Published 30 April 2019

DOI: [10.1103/PhysRevB.99.134520](https://doi.org/10.1103/PhysRevB.99.134520)

Surface terminations and layer-resolved tunneling spectroscopy of the 122 iron pnictide superconductors

Ang Li,^{1,3,9*} Jia-Xin Yin,^{2,1} Jihui Wang,¹ Zheng Wu,¹ Jihua Ma,^{1,4} Athena S. Sefat,⁵ Brian C. Sales,⁵ David G. Mandrus,⁵ Rongying Jin,⁶ Chenglin Zhang,⁷ Pengcheng Dai,⁷ Bing Lv,¹ Ching-Wu Chu,¹ Xuejin Liang,² P.-H. Hor,¹ C.-S. Ting,¹ and Shuheng H. Pan^{2,1,8,10,11*}

¹Department of Physics and Texas Center for Superconductivity, University of Houston, Houston, Texas 77204, USA

²Beijing National Laboratory for Condensed Matter Physics and Institute of Physics, Chinese Academy of Sciences, Beijing 100190, China

³State Key Laboratory of Functional Materials for Informatics, Shanghai Institute of Microsystem and Information Technology, Chinese Academy of Sciences, Shanghai 200050, China

⁴Department of Physics, Boston College, Chestnut Hill, Massachusetts 02467, USA

⁵Materials Science & Technology Division, Oak Ridge National Laboratory, Oak Ridge, Tennessee 37831, USA

⁶Department of Physics & Astronomy, Louisiana State University, Baton Rouge, Louisiana 70803, USA

⁷Department of Physics and Astronomy, Rice University, Houston, Texas 77005, USA

⁸School of Physics, University of Chinese Academy of Sciences, Beijing 100190, China

⁹CAS Center for Excellence in Superconducting Electronics, Shanghai 200050, China

¹⁰CAS Center for Excellence in Topological Quantum Computation, University of Chinese Academy of Sciences, Beijing 100190, China

¹¹Songshang Lake Material Laboratory, Dongguan, Guangdong 523808, China

*Corresponding authors: angli@mail.sim.ac.cn; span@iphy.ac.cn

Subject Areas: Condensed Matter Physics, Superconductivity

Abstract

The surface terminations of 122-type alkaline earth metal iron pnictides $AEFe_2As_2$ ($AE = Ca, Ba$) are investigated with scanning tunneling microscopy/spectroscopy (STM/STS). Cleaving these crystals at a cryogenic temperature yields a large majority of terminations with atomically resolved $(\sqrt{2} \times \sqrt{2})R45$ or 1×2 lattice, as well as a very rare termination of 1×1 lattice symmetry. By analyzing the lattice registration and selective chemical marking, we identify these terminations as $(\sqrt{2} \times \sqrt{2})R45$ -reconstructed AE , 1×2 -reconstructed As, and $(\sqrt{2} \times \sqrt{2})R45$ -reconstructed Fe surface layers, respectively. Layer-resolved tunneling spectroscopy on these terminating surfaces reveals a well-defined superconducting energy gap on the As terminations, while the gap features become weaker on the AE terminations and absent on the Fe terminations. The superconducting gap is hardly affected locally by the As or AE surface reconstructions. The definitive identification of the surface terminations and the associated spectroscopic signatures shed light on the essential roles of As and the pnictogen-iron-pnictogen trilayer building block in iron-based superconductivity.

I. INTRODUCTION

The discovery of iron-based superconductors marked a significant progress in the study of high-temperature superconductivity [1-3]. All iron-based superconductors share a unique pnictogen (chalcogen)-iron-pnictogen (chalcogen) trilayer structural unit, and it is generally believed that superconductivity develops primarily in the iron plane with $3d$ orbital characters [4]. To unravel the multi-orbital nature of the iron plane and to understand the roles of other ingredient layers, an atomic layer-resolved electronic characterization is thus essential. STM/STS is an ideal tool for extracting local structural and spectroscopic information. It has played a critical role in exploring the electronic interactions in iron-based superconductors [5]. So far, iron-based superconductors like Fe(Se,Te) and LiFeAs have been relatively well characterized by STM/STS due to their definitive crystal cleavage, while the study of 122-type alkaline earth metal iron pnictides $AEFe_2As_2$ ($AE = Ca, Ba, etc.$) suffers from controversial identifications of the cleavage planes due to the complex surface morphologies [6-23]. Therefore, clarification of the cleavage, identification of the resulting terminations, and subsequent layer-resolved spectroscopic investigations become crucial and highly demanded for studying the $AE122$ iron-based superconductivity.

Among iron-based superconductors, the $AE122$ compounds are noteworthy for their relatively high T_C and widely accessible chemical doping range [2,3]. They have a layered crystal structure with the weakest bonding between the adjacent AE and As layers (Fig. 1(a)). Accordingly, these crystals tend to cleave there between and the AE and As planes are most likely to be exposed as the surface terminations. As the adjacent As layer and AE layer are ionically bonded in bulk, upon cleaving, the unbalanced charge distribution on the terminations can lead to various surface reconstructions making the surface identification more complicated. Based on the early STM studies [6-23], two major assignments have been proposed for the $AE122$ -crystal surface terminations: (1) Upon cleaving, the AE atoms are divided statically into two 50% portions that redistribute uniformly onto the two adjacent As terminating surfaces to form either a $(\sqrt{2} \times \sqrt{2})R45$ or a 1×2 superstructure as a 50% AE -coverage [6-9,12,14,19-23]; (2) the AE atomic layer is disassembled into scattered atoms, clusters, or lumps instead of remaining in a complete atomic coverage layer, then the As layer is exposed with $(\sqrt{2} \times \sqrt{2})R45$ or 1×2 reconstruction [10,11,13,18]. In this article we present high-resolution STM/STS results on the cryogenically cleaved $AEFe_2As_2$ ($Ba(Fe_{1-x}Co_x)_2As_2$, $Ba_{1-x}K_xFe_2As_2$, and $CaFe_2As_2$) single crystals. We demonstrate that three types of ordered surface structure can be distinguished as (1) $(\sqrt{2} \times \sqrt{2})R45$ reconstruction of the complete AE lattice, (2) 1×2 stripes from the As dimerization, and (3) the rarely observed $(\sqrt{2} \times \sqrt{2})R45$ pattern of the Fe lattice. Local differential conductance measurements show superconducting gap features in the low-energy excitation spectra on both AE and As terminations, while not in that on the Fe exposure. Such

spectroscopic discrepancies indicate that the As-Fe-As trilayer structure is essential to the superconducting pairing in iron pnictides.

II. EXPERIMENTAL METHOD

The single crystalline samples of BaFe_2As_2 and CaFe_2As_2 with various doping were grown using the self-flux method [24-26]. In particular, the CaFe_2As_2 crystals were furnace-cooled to room temperature without quenching, thus no trace of low-temperature collapsed tetragonal phase was detected in the electrical resistivity and magnetic susceptibility measurements [27]. The STM/STS experiments were carried out on a home-built ultra-high vacuum low-temperature STM. Samples were cleaved *in situ* below 30 K and immediately transferred to the STM head which was already at the base temperature of 4.3 K. The scan tips were prepared from polycrystalline tungsten wires by electrochemical etching and subsequent field-emission cleaning. Topographic images were acquired in the constant-current mode with the bias voltage applied to the sample. Differential conductance spectra were recorded with the standard lock-in technique. When describing the lattice symmetry, we choose the ThCr_2Si_2 -type tetragonal notation throughout this article so that the low-temperature orthorhombic symmetry [28] can be denoted as " $(\sqrt{2}\times\sqrt{2})\text{R}45$ ", or "rt2" for short.

III. RESULTS AND DISCUSSION

The most commonly (about 99% of the time) observed surface terminations in AEFe_2As_2 resulted from cold cleaving are shown in Fig. 1(b) and Fig. 1(c). The 1×2 superstructure in Fig. 1(b) consists of one-dimensional stripes with inter-stripe distance $\sim 8 \text{ \AA}$, twice the tetragonal lattice constant. Along the stripe are grains at 4 \AA spacing and within each grain there are two atoms that can be resolved to form a dimer in high-resolution images (inset in Fig. 1(b)). This dimerization can follow either *a* or *b* direction, thus twin domain structures are often observed on a striped surface as shown in Fig. 1(b). The dimerization is most likely a surface phenomenon for no evidence has been reported from bulk measurements such as X-ray diffraction and high-resolution transmission electron microscope. The structural nature of the 1×2 symmetry is further evidenced by the independence of topographic image on the bias voltage. The second type of termination shown in Fig. 1(c) exhibits a bias-independent square-like lattice with a much smaller topographic corrugation. There, the unit cell is enlarged by $\sqrt{2}\times\sqrt{2}$ times from the tetragonal 1×1 base and orients at 45° to the 1×2 stripes (Fig. 2(a)). In such images, it seems that only 50% of the atoms in the atomic layer are resolved if one attempts to assign them to the *AE* or As layer. High resolution imaging, however, reveals the complete atomic coverage with a $\sqrt{2}\times\sqrt{2}$ buckling reconstruction (inset in Fig. 1(c)). Such a rt2 lattice reconstruction is consistently observed even in heavily overdoped $\text{Ba}(\text{Fe}_{1-x}\text{Co}_x)_2\text{As}_2$ samples, where the bulk low-temperature orthorhombic/magnetic phase is

completely suppressed [29]. Therefore, we conclude that the buckled $rt2$ superstructure is a surface phenomenon as well. In addition to 1×2 and $rt2$, a third type of surface morphology with 1×1 lattice symmetry (Fig. 1(d)) is very rarely observed. Knowing the easy cleavage plane lies between the AE and As layers, we expect the commonly observed 1×2 and $rt2$ surfaces are associated with the AE and/or As terminations exposed after cold cleaving.

As the AE and As layers share the same crystal lattice symmetry in the bulk, it is not decisive to assign the atomic identity of the 1×2 or $rt2$ reconstructed surface merely based on the structural symmetry. Due to the fact that the constant current topographic image convolutes the spatial variation of the integrated local density of states (LDOS) and the geometrical corrugations, simply assigning these terminations by their apparent image height would not be appropriate either. As an example, on a cleaved CaFe_2As_2 crystal, while the apparent step height between two stripe surfaces is consistent with the crystallographic dimension of a half unit cell $c/2$ (Fig. 2(a)), the apparent step height between a $rt2$ surface and a stripe surface in its STM image is one order of magnitude too small than any of the crystallographic spacings in the crystal (Fig. 2(b)). This clearly demonstrates that it is impossible to rely on the apparent step height in determination of the identities of two surfaces with different chemical identities or superstructures, not even to determine whether they are two different elemental terminations or simply the same elemental termination but with different surface reconstructions.

After carefully examining these topographic images and comparing with the crystal structures, we have developed a set of practical schemes to help in identifying these terminations. Firstly, we apply the relative lattice registration scheme and have noticed a critical clue from the in-plane lattice alignment between the adjacent 1×2 and $rt2$ regions in Fig. 3(a). Its zoom-in image in Fig. 3(b) clearly shows that the centerline of each stripe points in 45° exactly to the $rt2$ superlattice grid, indicating the two atomic lattices' half-unit-cell alignment. This observation supports the fact that the two commonly observed surface structures are not from the same atomic plane, but are associated with AE and As terminations respectively as shown in the schematic in Fig. 3(c). Secondly, we apply the selective doping scheme to determine their correspondence. As an example, we chose potassium to dope BaFe_2As_2 , in which potassium dopants partially substitute the Ba atoms [20]. In its $rt2$ topographic images (Fig. 3 (d) and (e)), bright and dark sites are readily visible at atomic level, while such contrast is absent in the 1×2 stripes. The percentage of dark sites is approximately 40%, agrees fairly well with the nominal concentration of K doping. This leads us to conclude that the two major surface terminations are created by cold cleaving between AE and As planes; the exposed AE layer buckles to form a $rt2$ -superstructure and the As atoms in arsenic plane dimerize to form one-dimensional stripes. Each of the two terminations alone does not cover

the entire cleaving surface. Instead, the entire surface is covered by a roughly 50%-50% mixture of them that are separated by single-atom-steps (Fig. 2(b)). The apparent step height of such single-atom-step in the STM topographic images is much smaller ($\sim 0.7\text{\AA}$ for BaFe_2As_2 and $\sim 0.1\text{\AA}$ for CaFe_2As_2) as compared to the crystalline AE -As interlayer distance (1.9\AA [28]), which can be explained by AE 's smaller contribution to the density of states near the Fermi level [30].

Having identified the commonly observed $rt2$ and 1×2 terminations, we then turn to the rare 1×1 termination (Fig. 1(d) and Fig. 3(f)). Considering its very low probability of occurrence, the 1×1 termination could be either an un-reconstructed version of the AE or As exposure [22,31] or the $(\sqrt{2}\times\sqrt{2})R45$ reconstructed pattern of the Fe lattice (whose original lattice constant is $1/\sqrt{2}$ times of that in As and AE). Again, we apply the lattice registration scheme. Note that the $rt2$ pattern of Fe, when surrounded by As stripes, should have a unique atomic registration with the As stripes from two orthogonal directions as illustrated in Fig. 3(g). There is a half-unit-cell shift in the alignment of $rt2$ Fe lattice with respect to the As stripes from a and b directions. We emphasize that this atomic lattice registration is exclusive for Fe terminations with $rt2$ reconstruction. The height profiles along two lines in Fig. 3(f) clearly demonstrate such a lattice registration with a half-unit-cell shift as highlighted in Fig. 3(h), which provides a decisive evidence of the 1×1 structure being the $rt2$ reconstructed pattern of the unusually exposed Fe layer.

The combination of low temperature cleaving and the definitive identification of all building layers provide one an extraordinary opportunity to perform layer-resolved spectroscopic investigations of $AE\text{Fe}_2\text{As}_2$. In Fig. 4, the spatially averaged differential conductance spectra on optimally doped $\text{Ba}(\text{Fe},\text{Co})_2\text{As}_2$ ($T_C \approx 22\text{ K}$) show the superconducting energy gap on both Ba and As terminations with the gap magnitude $\Delta \approx 6\text{ meV}$ and the ratio $2\Delta/k_B T_C \approx 6.3$, indicating a strong coupling superconducting state. Interestingly, the gap features are well defined in 1×2 As surface, while the spectrum on Ba termination exhibits reduced coherence peaks and more in-gap states near the Fermi level, probably caused by impurity scattering effect of Co doping. The cause of such spectral differences is still an open question, and we discuss this phenomenon in detail from the orbital perspective [32].

In strong contrast, the Fe termination is characterized by an overall V-shaped spectrum without features of superconductivity. This is quite puzzling as that even if there is no coherent Cooper pairing in the exposed Fe layer due to missing of the As coverage, there should still be a superconducting gap feature from the proximity of superconducting layers lying below. A possible scenario is that a metallic state co-exists in the region (caused by the surface termination/reconstruction) and obscures the observation of the proximity induced superconducting gap. If this is the case, then why this metallic state

is immune to the proximity effect needs an explanation. A possibility along another line is that magnetism can suppress the phase coherence of Cooper pairs [33], thus it is conceivable that without coverage of As, the Fe-terminated surface possesses strong magnetism that destroys the superconducting phase coherence. If this is the case, one should still see a gap-like DOS depression without coherent peaks in the tunneling spectrum, but this feature is absent. In any case, the V-shaped spectrum without any superconducting gap features on exposed Fe surface compared with the coherent gap spectrum on As surface essentially highlights the role of As layer and the vital integrity of the As-Fe-As tri-layered block in the electronic pairing and the emergence of superconductivity. Indeed, the magnetic and electronic properties depend very sensitively on the Fe-As local structures [34,35]. Removing the As layer can dramatically alter the coordination environment of Fe hence the pairing of electrons.

In addition to the chemical identity, the lattice reconstruction can also influence the surface electronic structure by inducing band folding in the momentum space. Our previous photoemission measurement shows that the 1×2 surface reconstruction leads to a noticeable band folding, with the band around Γ and M point of the Brillion zone being folded to the X position [36]. In our experimental observations, the representative broken symmetry in *AE* and As terminations, however, does not alter the low-energy local DOS spectrum significantly. For example, no perceivable change in the gap size is detected with 1×2 periodicity (Fig. 5(a) and (b)), except that the width of the coherence peaks is very weakly modulated across the stripe (Fig. 5(d)). This is consistent with the fact that the superconducting coherence length (typically more than 20\AA [7,16]) is much larger than the periodicities of these superlattices.

IV. SUMMARY

We have performed an STM/STS study on the *AE*-122 iron pnictides. Cleaving at a cryogenic temperature exposes the predominant rt_2 -buckled *AE* termination and 1×2 -dimerized As termination. Very occasionally the crystal cleaves between the As and Fe layers leaving the rt_2 reconstructed pattern of the Fe layer exposed with characteristic 1×1 lattice symmetry. The superconducting energy gap is observed on *AE* and As terminations, while no gap features are found on the Fe termination. Our atomic layer-resolved spectroscopic study suggests that the As-Fe-As trilayer block is essential for the superconductivity in 122 pnictides. The definite identification of various terminating surfaces and detailed spectroscopic characterization on each termination provide us valuable information towards a comprehensive understanding of the iron-based superconductivity. Our methodology of atomic surface identification and layer-revolved tunneling demonstrated here can also be generally applied to study other complex layered quantum materials [37, 38].

Acknowledgments

We sincerely thank Dr. Donghui Lu for helpful discussions. This work is supported by State of Texas through TcSUH, Chinese Academy of Sciences, NSFC (11227902, 11322432, 11190020), the Strategic Priority Research Program B (XDB04040300, XDB07000000) and the Hundred Talents Program of the Chinese Academy of Sciences, Ministry of Science and Technology of China (2012CB933000, 2012CB821400, 2015CB921300), and U.S. DOE (DE-SC0012311).

- [1] Y. Kamihara, T. Watanabe, M. Hirano, and H. Hosono, *J. Am. Chem. Soc.* 130, 3296 (2008).
- [2] D. Johnston, *Advances in Physics* 59, 803 (2010).
- [3] G. Stewart, *Reviews of Modern Physics* 83, 1589 (2011).
- [4] K. Juroki, S. Onari, R. Arita, H. Usui, Y. Tanaka, H. Kontani, and H. Aoki, *New J. Phys.* 11, 025017 (2009).
- [5] J. E. Hoffman, *Rep. Prog. Phys.* 74, 124513 (2011).
- [6] M. Boyer, K. Chatterjee, W. Wise, G. Chen, J. Luo, N. Wang, and E. Hudson, arXiv:0806.4400.
- [7] Y. Yin, M. Zech, T. Williams, X. Wang, G. Wu, X. Chen, and J. Hoffman, *Phys. Rev. Lett.* 102, 097002 (2009).
- [8] D. Hsieh, Y. Xia, L. Wray, D. Qian, K. Gomes, A. Yazdani, G. Chen, J. Luo, N. Wang, and M. Hasan, arXiv:0812.2289 (2008).
- [9] F. Massee, Y. Huang, R. Huisman, S. de Jong, J. Goedkoop, and M. Golden, *Phys. Rev. B* 79, 220517 (2009).
- [10] V. Nascimento, A. Li, D. Jayasundara, Y. Xuan, J. O'Neal, S. Pan, T. Chien, B Hu, X. He, G. Li, A. Sefat, M. McGuire, B. Sales, D. Mandrus, M. Pan, J. Zhang, R. Jin, and E. Plummer, *Phys. Rev. Lett.* 103, 076104 (2009).
- [11] F. Niestemski, V. Nascimento, B. Hu, W. Plummer, J. Gillett, S. Sebastian, Z. Wang, and V. Madhavan, arXiv:0906.2761(2009).
- [12] F. Massee, S. de Jong, Y. Huang, J. Kaas, E. van Heumen, J. Goedkoop, and M. Golden, *Phys. Rev. B* 80, 140507 (2009).
- [13] T. Chuang, M. Allan, J. Lee, Y. Xie, N. Ni, S. Bud'ko, G. Boebinger, P. Canfield, and J. Davis, *Science* 327, 181 (2010).
- [14] H. Zhang, J. Dai, Y. Zhang, D. Qu, H. Ji, G. Wu, X. Wang, X. Chen, B Wang, C. Zeng, J. Yang, and J. Hou, *Phys. Rev. B* 81, 104520 (2010).
- [15] T. Nishizaki, Y. Nakajima, T. Tamegai, and N. Kobayashi, *J. Phys. Soc. Jpn.* 80, 014710 (2011).

- [16] L. Shan, Y. Wang, B. Shen, B. Zeng, Y. Huang, A. Li, D. Wang, H. Yang, C. Ren, Q. Wang, S. Pan, and H. Wen, *Nature Physics* 7, 325 (2011).
- [17] M. Teague, G. Drayna, G. Lockhart, P. Cheng, B. Shen, H. Wen, and N. Yeh, *Phys. Rev. Lett.* 106, 087004 (2011).
- [18] G. Li, X. He, J. Zhang, R. Jin, A. Sefat, M. McGuire, D. Mandrus, B. Sales, and E. Plummer, *Phys. Rev. B* 86, 060512 (2012).
- [19] K. Koepf, S. Johnston, E. van Heumen, Y. Huang, J. Kaas, J. B. Goedkoop, M. S. Golden, and J. Brink, *Phys. Rev. Lett.* 109, 127001 (2012).
- [20] Z. Wang, H. Yang, D. Fang, B. Shen, Q. Wang, L. Shan, C. Zhang, P. Dai, and H. Wen, *Nature Physics* 9, 42 (2013).
- [21] I. Zeljkovic, D. Huang, C. Song, B. Lv, C. Chu, and J. Hoffman, *Phys. Rev. B* 87, 201108 (2013).
- [22] C. Song, Y. Yin, M. Zech, T. Williams, M. Yee, G. Chen, J. Luo, N. Wang, E. Hudson, and J. Hoffman, *Phys. Rev. B* 87, 214519 (2013).
- [23] G. Li, L. Liang, Q. Li, M. Pan, V. B. Nascimento, X. He, A. B. Karki, V. Meunier, R. Jin, J. Zhang, and E. W. Plummer, *Phys. Rev. Lett.* 112, 077205 (2014).
- [24] A. Sefat, R. Jin, M. McGuire, B. Sales, D. Singh, and D. Mandrus, *Phys. Rev. Lett.* 101, 117004 (2008).
- [25] C. Zhang, M. Wang, H. Luo, M. Wang, M. Liu, J. Zhao, D. L. Abernathy, T. A. Maier, K. Marty, M. D. Lumsden, S. Chi, S. Chang, J. A. Rodriguez-Rivera, J. W. Lynn, T. Xiang, J. Hu, and P. Dai, *Scientific Report* 1, 115 (2011).
- [26] B. Lv, L. Deng, M. Gooch, F. Wei, Y. Sun, J. K. Meen, Y. Xue, B. Lorenz, and C.-W. Chu, *Proc. Natl. Acad. Sci. USA* 108, 15705 (2011).
- [27] S. Ran, S. L. Bud'ko, D. K. Pratt, A. Kreyssig, M. G. Kim, M. J. Kramer, D. H. Ryan, W. N. Rowan-Weetaluktuk, Y. Furukawa, B. Roy, A. I. Goldman, and P. C. Canfield, *Phys. Rev. B* 83, 144517 (2011).
- [28] M. Rotter, M. Tegel, D. Johrendt, I. Schellenberg, W. Hermes, and R. Pöttgen, *Phys. Rev. B* 78, 020503 (2008).

- [29] N. Ni, M. Tillman, J. Yan, A. Kracher, S. Hannahs, S. Bud'ko, and P. C. Canfield, *Phys. Rev. B* 78, 214515 (2008).
- [30] I. Shein and A. Ivanovskii, *JETP* 88,107-110 (2009).
- [31] M. Gao, F. Ma, Z. Lu, and T. Xiang, *Phys. Rev. B* 81, 193409 (2010).
- [32] J.-X. Yin, Ang Li, X. -X. Wu, Jian Li, Zheng Wu, J.-H. Wang, C.-S. Ting, P.-H. Hor, X. J. Liang, C. L. Zhang, P. C. Dai, X. C. Wang, C. Q. Jin, G. F. Chen, J. P. Hu, Z. -Q. Wang, H. Ding, S. H. Pan, *arXiv:1602.04949* (2016).
- [33] A. V. Balatsky, I. Vekhter, J.-X. Zhu, *Rev. Mod. Phys.* 78, 373–433 (2006).
- [34] Z. Yin, K. Haule, and G. Kotliar, *Nature Materials* 10, 932 (2011).
- [35] C. Zhang, L. W. Harriger, Z. Yin, W. Lv, M. Wang, G. Tan, Y. Song, D. L. Abernathy, W. Tian, T. Egami, K. Haule, G. Kotliar, and P. Dai, *Phys. Rev. Lett.* 112, 217202 (2014).
- [36] Y. Huang, R. Pierre, J. Wang, X. Wang, X. Shi, N. Xu, Z. Wu, A. Li, J. Yin, T. Qian, B. Lv, C. Chu, S. Pan, M. Shi, and H. Ding, *Chin. Phys. Lett.* 30, 017402 (2013).
- [37] J-X. Yin, Zheng Wu, J-H. Wang, Z-Y. Ye, Jing Gong, X-Y. Hou, Lei Shan, Ang Li, X-J. Liang, X-X. Wu, Jian Li, C-S. Ting, Z-Q. Wang, J-P. Hu, P-H. Hor, H. Ding, and S. H. Pan, *Nature Physics* 11, 543–546 (2015).
- [38] Jia-Xin Yin, Songtian S. Zhang, Hang Li, Kun Jiang, Guoqing Chang, Bingjing Zhang, Biao Lian, Cheng Xiang, Ilya Belopolski, Hao Zheng, Tyler A. Cochran, Su-Yang Xu, Guang Bian, Kai Liu, Tay-Rong Chang, Hsin Lin, Zhong-Yi Lu, Ziqiang Wang, Shuang Jia, Wenhong Wang & M. Zahid Hasan, *Nature* 562, 91-95 (2018).

Figures:

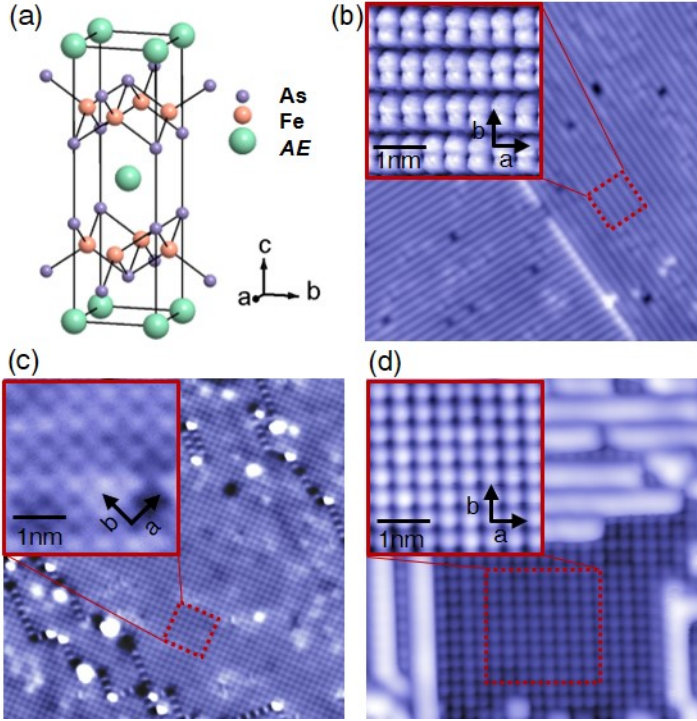


FIG. 1: (a) Schematic crystal structure of $AEFe_2As_2$. (b-d) Surface morphologies demonstrating (b) 1×2 ($V = 100$ mV, $I = 30$ pA), (c) $rt2$ ($V = 20$ mV, $I = 2$ nA), and (d) 1×1 ($V = 50$ mV, $I = 2$ nA) superstructures. Insets in (b-d) are the zoom-in image of 1×2 dimers ($V = 20$ mV, $I = 8$ nA), $rt2$ buckling ($V = 20$ mV, $I = 2$ nA) and 1×1 surface ($V = 50$ mV, $I = 2$ nA), respectively.

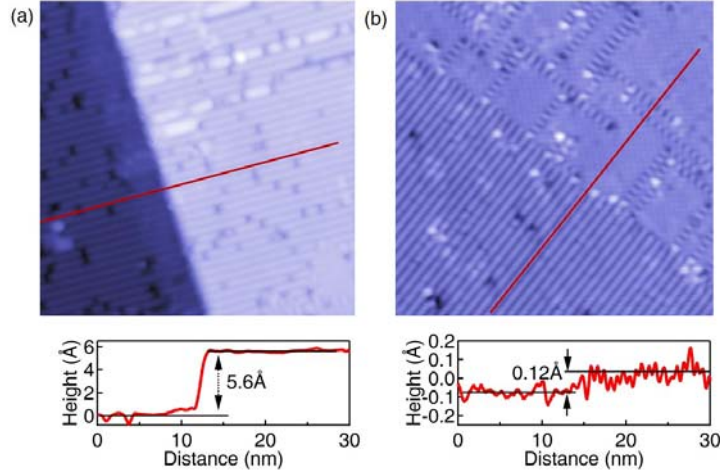


FIG. 2 (a) The step height of $\sim 5.6\text{\AA}$ between two stripe surfaces, which is consistent with the crystallographic dimension of a half unit cell $c/2=5.8\text{\AA}$. (b) The step between a rt_2 surface and a stripe surface with the apparent step height of $\sim 0.12\text{\AA}$, that is one order of magnitude too small than any of the crystallographic spacing in this crystal. For both cases, the topological profile along the line marked in the upper topographic image is shown in the lower panel. Data are both taken in CaFe_2As_2 at 4.2K for an area of $300\times 300\text{\AA}^2$ with tunneling junction set up: $V = 50\text{ mV}$, $I = 0.5\text{ nA}$.

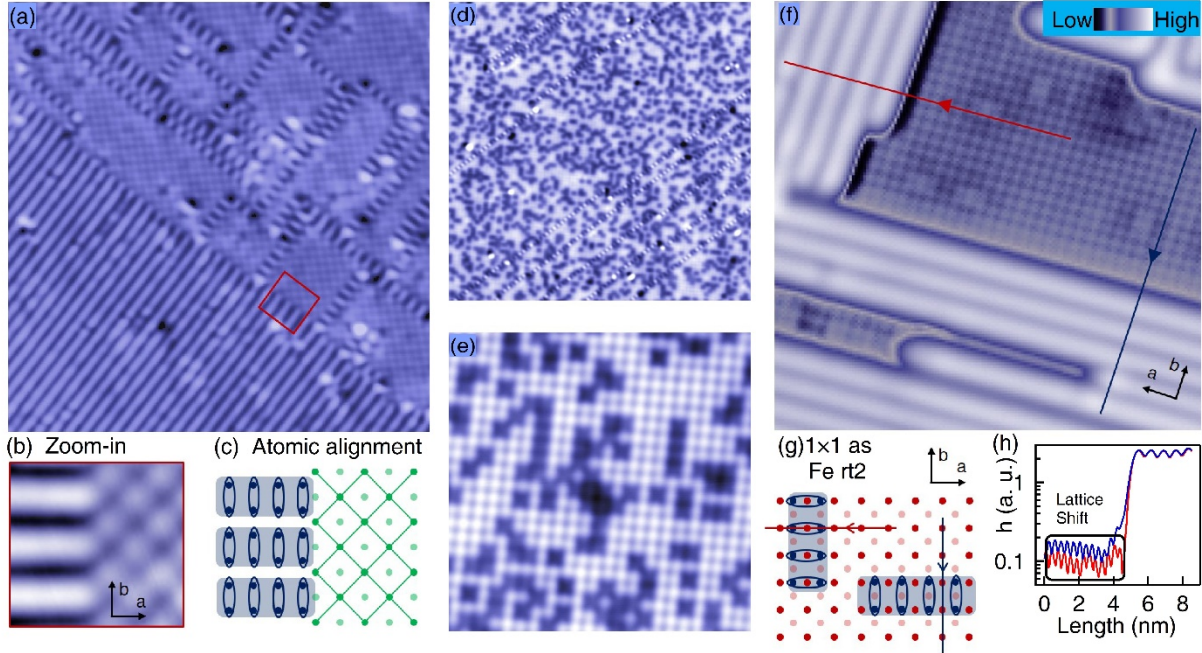


FIG. 3: (a) The joint area between rt2 and 1×2 in CaFe_2As_2 ($400\times 400 \text{ \AA}^2$, $V = 50 \text{ mV}$, $I = 1 \text{ nA}$). (b) The zoom-in images of boundaries as marked in the red box in (a). (c) Schematic drawings for the in-plane atomic lattice registration at joint boundary of 1×2 and rt2 areas when they belong to two different atomic layers (As and AE). Ellipses and solid lines represent the dimers and rt2 superlattice respectively. The rt2 topographies of $\text{Ba}_{0.6}\text{K}_{0.4}\text{Fe}_2\text{As}_2$ are shown in (d) $500\times 500 \text{ \AA}^2$, $V = -100 \text{ mV}$, $I = 2 \text{ nA}$ and (e) $125\times 125 \text{ \AA}^2$, $V = 100 \text{ mV}$, $I = 2 \text{ nA}$. (f) 1×1 area surrounded by the 1×2 stripes in CaFe_2As_2 ($130\times 130 \text{ \AA}^2$, $V = 50 \text{ mV}$, $I = 1 \text{ nA}$). (g) Schematic drawings for the in-plane atomic arrangement of stripes vs 1×1 lattice assuming that 1×1 is rt2-buckled Fe (As: dark blue, Fe: dark and light red). (h) Height profiles along the 1×1 lattice in orthogonal directions indicated in (f). A half-unit-cell lattice shift in the 1×1 profile relative to the stripe profile can be clearly observed.

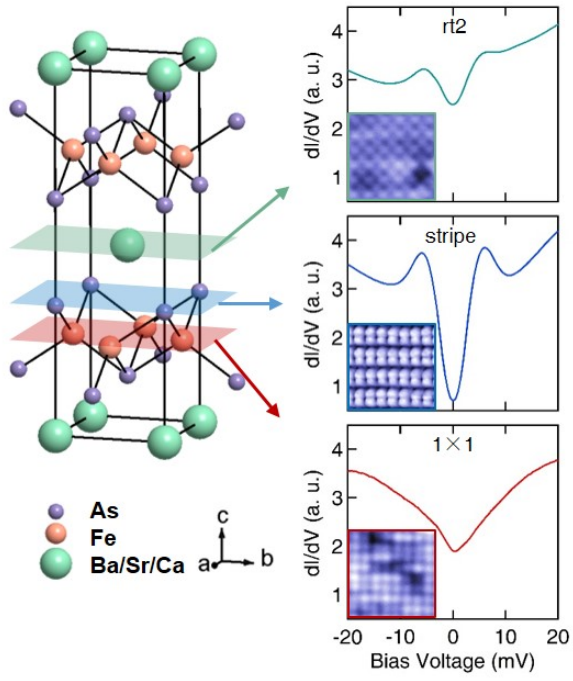


FIG. 4: Spatially averaged differential conductance spectra on three surface terminations in optimally doped $\text{Ba}(\text{Fe,Co})_2\text{As}_2$ ($V = -20$ mV, $I = 0.67$ nA). The insets show the corresponding topographic images with the size of $35 \times 35 \text{ \AA}^2$

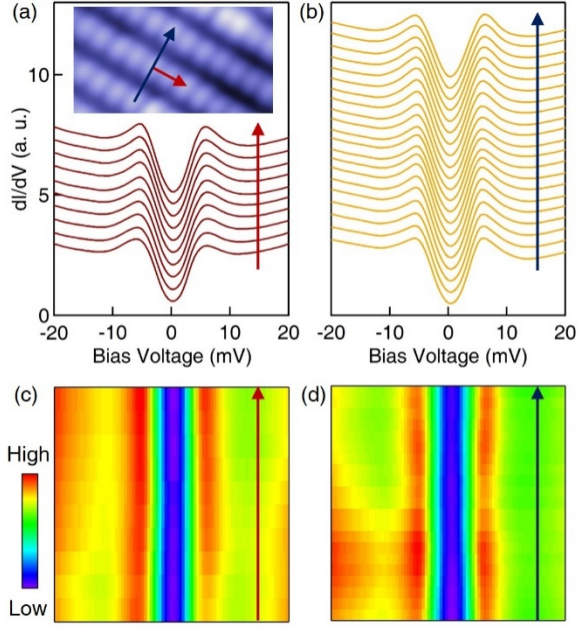


FIG. 5: (a) and (b) Series of differential conductance spectra measured along and across the As stripes for optimally doped $\text{Ba}(\text{Fe},\text{Co})_2\text{As}_2$ ($V = -20$ mV and $I = 0.67$ nA). The trajectories are drawn in the inset of (a). Spectra are offset for clarity. The inset image shows the corresponding topographic image with the size of $25 \times 50 \text{ \AA}^2$. (c) and (d) Intensity plot of the spectra in (a) and (b) respectively.